Article

Redox State of Cytochromes in Frozen Yeast Cells Probed by Resonance Raman Spectroscopy

Konstantin A. Okotrub[1] and Nikolay V. Surovtsev[1,2,*]
[1]Institute of Automation and Electrometry, Russian Academy of Sciences, Novosibirsk, Russia; and [2]Novosibirsk State University, Novosibirsk, Russia

ABSTRACT Cryopreservation is a well-established technique used for the long-term storage of biological materials whose biological activity is effectively stopped under low temperatures (suspended animation). Since most biological methods do not work in a low-temperature frozen environment, the mechanism and details of the depression of cellular activity in the frozen state remain largely uncharacterized. In this work, we propose, to our knowledge, a new approach to study the downregulation of the redox activity of cytochromes *b* and *c* in freezing yeast cells in a contactless, label-free manner. Our approach is based on cytochrome photobleaching effects observed in the resonance Raman spectra of live cells. Photoinduced and native redox reactions that contributed to the photobleaching rate were studied over a wide temperature range (from −173 to +25°C). We found that ice formation influences both the rate of cytochrome redox reactions and the balance between the reduced and oxidized cytochromes. We demonstrate that the temperature dependence of native redox reaction rates can be well described by the thermal activation law with an apparent energy of 32.5 kJ/mol, showing that the redox reaction rate is ~10^{15} times slower at liquid nitrogen temperature than at room temperature.

INTRODUCTION

Although cryopreservation techniques play a crucial role in biological studies, medicine, and industry (1–4), our knowledge about the effects of extreme cryoprotection conditions on cells remains limited, and the development of experimental techniques to measure cellular activity under cryopreservation is of great importance. Suspended animation in cryopreserved samples is achieved via depression of biochemical reactions by low temperatures (5) and high viscosity of the frozen matter. The depression of cellular activity preserves the cell and simultaneously protects it from the extreme environment around the cryopreserved sample.

Since cellular activity is accompanied by energy generation, it is closely interrelated with cellular respiration, including the operation of the electron transport chain (ETC). Unfortunately, the effects of low temperatures and the transition of freezing cells into a suspended-animation state on cellular respiration processes are not well understood. Although several studies have demonstrated the depression of respiration activity in cells thawed from the frozen state (6–9), how respiration activity changes during cryopreservation remains elusive.

A number of experimental techniques are used to study cellular respiration under physiological conditions; however, most of them have to be carried out at temperatures above those required for extracellular ice formation (6–8,10). Direct respiration measurements (11–13) are not suitable for low-temperature studies in which cells are trapped in a solid matrix. Contactless experimental techniques, such as optical spectroscopy methods, are considered methods of choice for low-temperature respiration studies (12,14–16). However, changes in the optical quality of the sample and the temperature dependence of the fluorescence efficiency significantly restrict the capabilities of optical methods that are based on acquiring an absolute signal.

Raman spectroscopy is a contactless technique that has been used successfully to study ice distribution (17), eutectic crystallization (18,19), and cryoprotector concentrations (17) within and around frozen cells. A powerful capability of Raman spectroscopy relates to the resonance-scattering effect of heme-containing proteins. Notably, resonance Raman spectroscopy can provide information about both the cytochrome redox state (20–23) and the cytochrome distribution (21–25).

Recently, an approach that measures redox reaction rates based on the photobleaching effect of cytochrome resonance Raman lines was proposed (26). In this approach, laser radiation excites the resonance Raman scattering and therefore allows one to quantify the amount of the reduced cytochromes. Simultaneously, irradiation changes the cytochrome redox balance in the cell via photoinduced oxidation processes. This photoinduced oxidation decreases the amount of reduced cytochromes and results in photobleaching of the resonance Raman lines. The photobleaching rate of the resonance Raman lines versus the irradiation power can be described by a square function plus a constant, where the square part

Submitted June 26, 2015, and accepted for publication October 26, 2015.
*Correspondence: lab21@iae.nsk.su
Editor: Leonid Brown.

0006-3495/15/12/2227/8
http://dx.doi.org/10.1016/j.bpj.2015.10.033

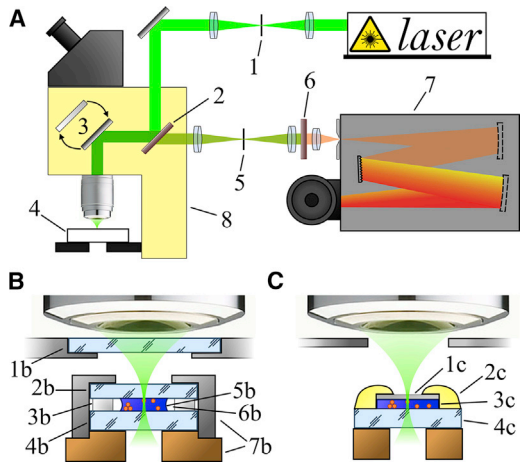

FIGURE 1 Experimental setup and sample installations in the two cryostages. (*A*) Experimental setup: 1) spatial filter with a 90 μm pinhole, 2) dichroic beam splitter, 3) switchable mirrors, 4) sample placed in cryostat, 5) spatial filter with a 120 μm pinhole, 6) edge filter, 7) spectrometer, and 8) microscope. (*B*) Sample installation in the vacuum cryostat: 1b) lid window (280 μm), 2b) top sample window (280 μm), 3b) Teflon ring, 4b) bottom sample window (~1 mm), 5b) cell suspension, 6b) air separating the sample (5b) from the Teflon ring, and 7b) metal casing. (*C*) Sample installation in the Linkam cryostage: 1c) mica slice (~10 μm), 2c) paraffin, 3c) cell suspension, and 4c) silica glass plate. To see this figure in color, go online.

is responsible for the photoinduced processes and the constant is responsible for the native cytochrome redox reactions (26). Therefore, resonance Raman spectroscopy can be used to characterize the native cytochrome reaction rates of the ETC.

In this work, we studied the redox state of cytochromes *b* and *c* in frozen yeasts using time-resolved resonance Raman experiments. A detailed investigation of the cytochrome photobleaching effect allowed us to evaluate the rate of cytochrome redox reactions in the ETC of frozen yeast cells for a wide range of temperatures.

MATERIALS AND METHODS

Sample preparation

Samples were prepared by adding 20 mg of *Saccharomyces cerevisiae* instant yeast cell pellets (Instant Dry Yeast; Pakmaya) to 5 mL of an isotonic saline solution.

In addition, a special experiment was performed at a high salt concentration. For this purpose, cells were suspended in a hypertonic solution (25 wt % NaCl) that was prepared by gradually increasing the salt concentration.

Raman experiment

We used a laboratory-built Raman setup (see Fig. 1) based on a modified microscope (Orthoplan, Leitz) and a monochromator (SP2500i; Princeton Instruments) equipped with a CCD detector (Spec-10:256E/LN; Princeton Instruments). We calibrated the spectrometer wavelength using a neon-discharge lamp. The spectral resolution was ~2.5 cm^{-1}. A solid-state laser (Millennia II; Spectra Physics) at a wavelength of 532.1 nm was used for Raman scattering excitation, and the beam power was measured with a photodiode power meter (Lasercheck; Coherent). Irradiation was focused on an ~1 μm spot of the sample using a 100× air objective with NA = 0.75 and a working distance of 4.6 mm (PL FLUOTAR L; Leica Microsystems). A system of switchable mirrors was used to switch between the sample observation and Raman acquisition modes. An edge filter (LP03-532RE-25; Semrock) was used to suppress the elastically scattered light by six orders of magnitude.

Two microscope cryostats (an in-house-made vacuum cryostat and a Linkam cryostage (FTIR600; Linkam)) were used, and both devices were continuously cooled by the flow of liquid nitrogen vapor as the refrigerant. The vacuum cryostat offers minimal sample vibrations at operating temperatures ranging from −195 to +40°C. The Linkam cryostage with the lid window removed provides higher Raman signal compared with the vacuum cryostat, but it can only be used at temperatures above −30°C. To avoid water condensation, the cryostage was purged by dry nitrogen and partially isolated from room air by a plastic cylinder. The container used in the vacuum cryostat provided sample aeration (Fig. 1 *B*), whereas the container used in the Linkam cryostage did not (Fig. 1 *C*).

In Raman scattering experiments, a single cell was exposed to a constant power of the laser beam. The sequence of Raman spectra (up to 40 scans) was measured at an integration time optimized for a particular photobleaching rate (which varied from 2 s to 2 min for different temperatures). For every experimental condition of the time-resolved Raman experiment, 10–40 cells were analyzed.

Sample freezing

The vacuum cryostat has good thermal isolation and can be used successfully in a wide range of temperatures. For experiments using the vacuum cryostat setup, a drop of the cell suspension (~1 μL) was placed into a hermetic sandwich between two silica glass plates and a Teflon ring (Fig. 1 *B*). A sample droplet was separated from the Teflon ring by air, resulting in sample aeration. Vacuum sealing of the sandwich was achieved via the metal housing. The temperature of the sample holder was monitored via a thermocouple and stabilized with a PID controller. Spontaneous extracellular ice formation was detected by visual observation. When the vacuum cryostat was used, spontaneous ice nucleation was observed in the temperature range from −15°C to −20°C.

In experiments with the Linkam cryostage, the cell suspension was placed on a fused silica slide, covered with a piece of mica, and sealed with paraffin (see Fig. 1 *C*). The suspension had no contact with air, and thus the samples were nonaerated. The sample-holder temperature was measured and manipulated with the use of a controller (T95; Linkam). The flow of liquid nitrogen vapor was minimal to maintain the set temperature. This cryostage was used in a temperature range of +25°C to −30°C. Spontaneous ice formation was observed in a temperature range of −5°C to −10°C.

All experiments were carried out at a cooling rate of 1–2°C/min, which corresponds to a high probability of yeast survival (27). This cooling rate is believed to be slow enough to provide effective yeast cell dehydration. In agreement with this, we observed cell shrinking in our experiments.

After ice formation was observed, Raman scattering was measured from single cells trapped in ice without neighbors. The temperature in the irradiated area of the cell was additionally controlled by the position of the ice Raman peak at ~3100 cm^{-1}. Representative Raman spectra of ice can be found elsewhere (18). Importantly, the position of the ice Raman peak shows a significant temperature dependence, which can be used to estimate the actual cell temperature. In the vacuum cryostat, laser overheating was estimated to be approximately or less than 3°C (compared with the average sample temperature measured by the thermocouple). When the Linkam cryostage with the lid window removed was used, the difference between the temperatures measured by the sensor and those estimated from the Raman spectra reached 10°C at the lowest temperature. The temperature extracted from the ice Raman peak position was used as the actual temperature of the frozen samples.

RESULTS

Temperature dependence of the cytochrome resonance Raman lines' intensity

The Raman spectrum of yeast cells measured with a 532 nm laser excitation contains a contribution from the resonance Raman lines of cytochromes. The contribution of the cytochrome lines decreases with the laser exposition (26). Representative Raman spectra of the yeast cells at room temperature and in the frozen state (–100°C) measured at the beginning and end of irradiation exposure are shown in Fig. 2. All Raman spectra of yeast cells consist of the same set of lines. Here, the Raman modes of interest are the CH deformation mode (δCH) at 1450 cm^{-1} and the resonance Raman lines of cytochromes *b* and *c* (749, 1129, and 1586 cm^{-1}) (28) (for detailed line assignments, see Table S1 in the Supporting Material). The intensity of the cytochrome Raman lines depends on the resonance enhancement, which is high for the reduced cytochrome state (Fe^{2+}) and is lower by a few orders of magnitude for the oxidized cytochrome (Fe^{3+}) (20). Therefore, the Raman intensity of the cytochrome lines can be used to evaluate the amount of reduced cytochromes.

As shown in Fig. 2, the intensity of the cytochrome lines decreases under irradiation (see also Fig. S3). This photobleaching effect is caused by the photoinduced cytochrome oxidation, and the photobleaching rate depends on the temperature. To evaluate the temperature dependence of the photobleaching, we measured time-resolved Raman spectra at each temperature.

The line at 749 cm^{-1} corresponding to the heme pyrrole rings' breathing mode (28) was chosen to characterize the cytochrome's contribution to the Raman spectrum. Since absolute Raman intensity measurements are prone to systematic errors, the intensity ratio of the line at 749 cm^{-1} (I_{749}) and of the δCH mode ($I_{\delta CH}$) was considered. According to Hu et al. (28), the δCH mode does not overlap with the resonance modes of the cytochrome heme. The method used to calculate the $I_{749}/I_{\delta CH}$ ratio is described in Supporting Materials and Methods.

The photobleaching response was described using an exponential decay fit (26):

$$\frac{I_{749}}{I_{\delta CH}} = y_0 + (A - y_0) \times e^{-t/\tau}, \quad (1)$$

where τ is the photobleaching time, the y_0 constant is proportional to a stationary amount of the reduced cytochromes under irradiation, and A is the initial ratio, which is proportional to the amount of reduced cytochromes without irradiation.

We determined the parameters of the photobleaching response from the fit of experimental data using Eq. 1. The temperature dependencies of the parameters A and y_0 are shown in Fig. 3, *A* and *B*, respectively. For these parameters, no significant temperature dependence was observed below the temperature of ice formation (T_{IF} ~ –15°C). The magnitudes of A and y_0 above T_{IF} depended on the freezing protocol. When the protocol with aeration of the sample was used, the contribution of the reduced cytochrome was low at high temperatures and increased below T_{IF} (Fig. 3, *A* and *B*). Notably, a similar increase was observed for the ATP concentration in *Psychrobacter cryohalolentis* that was incubated and thawed from temperatures below −15°C (10). When the sample was sealed without oxygen, it showed higher cytochrome contributions above T_{IF} (Fig. 3, *A* and *B*). In contrast, the magnitude of the cytochrome contribution was similar for aerated and nonaerated cells at

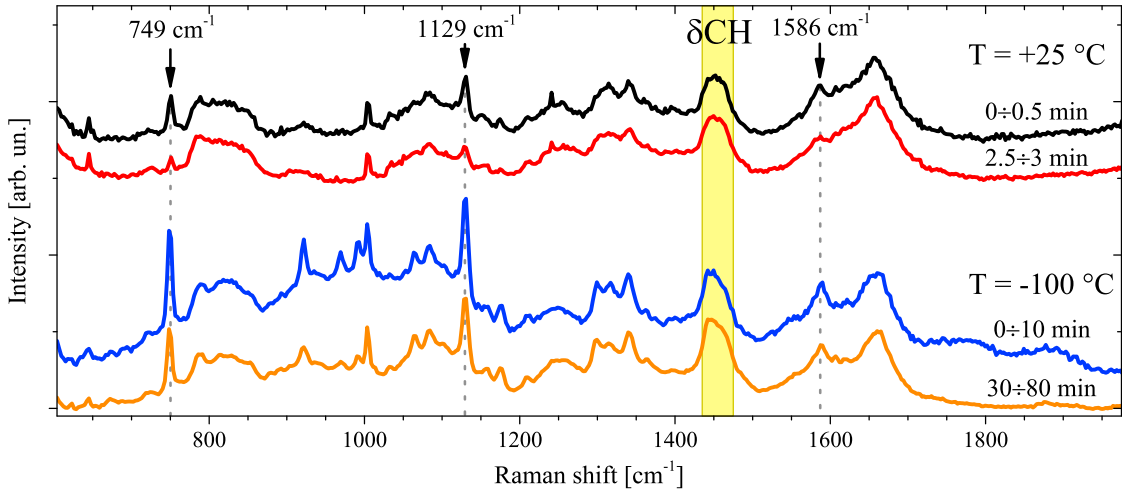

FIGURE 2 Raman spectra of yeast cells. The spectra are vertically shifted for convenience. Order of spectra (from *top* to *bottom*): yeast cells ($T = +25°C$) at the beginning of irradiation and after 2.5 min of irradiation exposure, and frozen yeast cells ($T = -100°C$) at the beginning of irradiation and after 30 min of exposure. The photoluminescence background was corrected in linear approximation. The arrows and vertical dashed lines denote Raman peaks of the cytochrome, and the shadow stripe marks the δCH mode. To see this figure in color, go online.

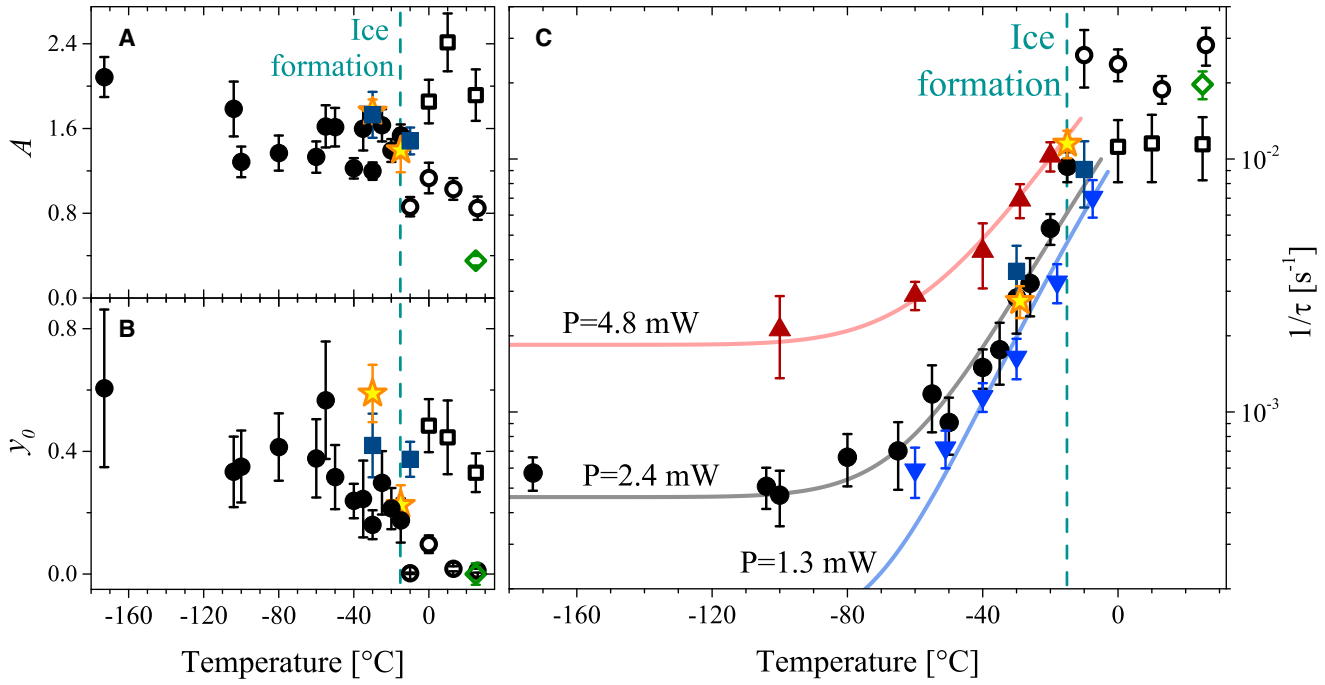

FIGURE 3 (*A–C*) Temperature dependencies of the fit parameters of Eq. 1: A (*A*), y_0 (*B*), and τ^{-1} (*C*). Data obtained using 2.4 mW irradiation for aerated (*circles*) and nonaerated (*squares*) samples are presented. Open symbols correspond to the ice-free solution and solid symbols represent the solution with extracellular ice. Yellow stars mark parameters determined for samples that were reheated after freezing. The green diamond denotes data obtained from 25 wt % NaCl. Up and down triangles correspond to τ^{-1} of the aerated samples under 4.8 mW and 1.3 mW of laser power, respectively. Solid lines were calculated as described in the text. Symbols represent mean ± SEM ($n \geq 10$). To see this figure in color, go online.

temperatures below T_{IF}. The effects of ice formation on the intensity of the cytochrome contribution were also directly observed in an additional experiment described in Supporting Materials and Methods (see Fig. S4).

The cytochrome photobleaching rate (τ^{-1}) did not show a significant temperature dependence above T_{IF} (Fig. 3 *C*). Samples that had access to oxygen showed higher photobleaching rates, indicating higher redox activity. The photobleaching rate gradually decreased below T_{IF} and reached a low-temperature plateau below −80°C (Fig. 3 *C*; note that a logarithmic scale is used for τ^{-1}). Since the photobleaching rate has a peculiar irradiation power dependence (26), the temperature dependence of τ^{-1} was studied in detail for three irradiation powers (Fig. 3 *C*). As expected, different photobleaching rates were observed for different powers. This difference can be well explained by the contributions from photoinduced and native redox reactions, which is further discussed in the next section.

Extracellular ice formation is known to increase the concentration of the solute. Therefore, the effects of extracellular ice formation seen in Figs. 3, *A–C*, and S4 could be due to an increase in the salt concentration around the yeast cells. If this were true, the increase in the salt concentration around yeast cells at room temperature would be expected to affect the photobleaching rate and cytochrome redox state in a manner similar to that observed for ice formation. To test this possibility, we studied the Raman spectra of the yeast cells in 25 wt % NaCl solution at $T = +25$°C (irradiation power 2.4 mW). Interestingly, we found that the high salt concentration had the opposite effect of ice formation, and the contribution of the reduced cytochrome was decreased when the high salt concentration was used (see Fig. 3, *A* and *B*). We suppose that the decreased contribution of the reduced cytochrome in cells in the hypertonic solution could be explained by the osmotic stress (29,30). No influence of the high salt concentration was found for τ^{-1} (Fig. 3 *C*). Thus, the effects of ice formation on the rate of cytochrome redox reactions and redox balance (Fig. 3, *A–C*) were not caused by the increased salt concentration around the yeasts.

To test whether the temperature effects presented in Fig. 3 were caused by irreversible freezing damage, we performed an experiment with yeasts reheated after freezing (freezing temperature: −100°C; irradiation power: 2.4 mW). The reheated yeasts demonstrated the same parameters as yeasts that were directly cooled to the reference temperature (Fig. 3), showing that the effect of temperature on the photobleaching rate did not result from irreversible freezing damage.

Cytochrome redox activity in freezing cells

Next, we used the photobleaching process to investigate cytochrome redox activity in the ETC of freezing cells. In

the framework of the model we proposed previously (26), the photobleaching response comes from photoinduced and native redox reactions. The rate of the photoinduced process has a quadratic dependence on the irradiation intensity. Native redox reactions are related to the operation of the ETC and run independently of the irradiation intensity. Thus, the power dependence of the photobleaching rate can be described as (26)

$$\tau^{-1}(P) = k_{dark} + \alpha P^2, \quad (2)$$

where k_{dark} is a constant related to the rate of native redox reactions, α is a coefficient of the photoinduced reaction, and P is the irradiation power.

Both items in Eq. 2 can be temperature dependent. To clarify their contributions to the observed temperature dependence of τ^{-1} (Fig. 3 *C*), we studied the irradiation power dependence of τ^{-1} at several different temperatures (Fig. 4). The power dependence observed at +25°C agreed with our previous results (26). In addition, the data obtained at −30°C, corresponding to the frozen sample, were well described by Eq. 2 (Fig. 4). We conclude that Eq. 2 is also valid at temperatures below T_{IF}. The power dependencies of τ^{-1} measured at different temperatures were fitted by Eq. 2 (Fig. 4). The temperature dependencies of k_{dark} and the α coefficient are shown in Fig. 5. The rate of the native reactions decreased with decreasing temperature and vanished in the limit of low temperatures. Therefore, the plateau in the temperature dependence of τ^{-1} below −80°C (Fig. 3 *C*) is associated with the photoinduced process.

The coefficient α determined from the fit by Eq. 2 also decreased when the temperature decreased. The second term in Eq. 2 could be a result of the direct two-photon absorption and/or a chemical reaction of the cytochrome with

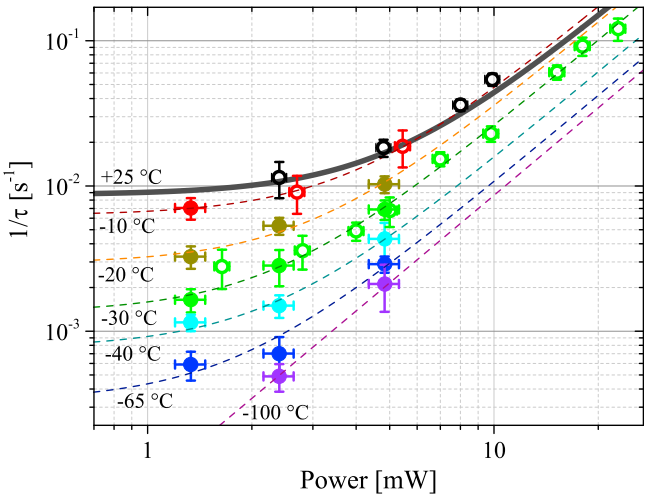

FIGURE 4 Irradiation power dependence of τ^{-1} at different temperatures. Solid and open circles correspond to aerated and nonaerated samples, respectively. Dashed lines are fits by Eq. 2. The thick solid line shows the power dependence obtained at $T = +25°C$ (26). Symbols represent mean ± SEM ($n \geq 10$). To see this figure in color, go online.

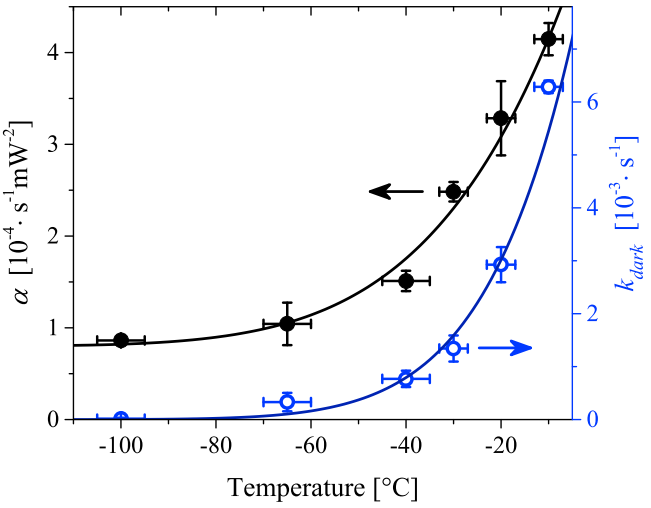

FIGURE 5 Temperature dependencies of the α coefficient (*solid circles*, *left axis*) and k_{dark} (*empty circles*, *right axis*). Solid lines are fits by the thermal activation law for k_{dark} and by the sum of the thermal activation law and a constant for α. Error bars denote standard error. To see this figure in color, go online.

two molecules of the intermediates released in photoreactions (26). Both scenarios lead to a quadratic power dependence. A finite τ in the solid surroundings ($T = -173°C$; Fig. 3 *C*) implies a localization of the photobleaching processes within the low-temperature limit. On the other hand, $\alpha(T)$ showed a fourfold decrease in the temperature range of −10 to −65°C (Fig. 5), which is inconsistent with local two-photon-like processes only. We hypothesize that at least two different channels contribute to the photoinduced item in Eq. 2. The first channel is localized and temperature independent, whereas the second channel can be described by the thermal activation law. The activation energy of $\alpha(T)$, 21.3 (±15%) kJ/mol, was determined from the fit (Figs. 5 and S5).

The temperature dependence of k_{dark} extracted from the photobleaching experiment is shown in the Arrhenius plot in Fig. 6. This temperature dependence can be well described by the thermal activation law with an activation energy of 32.5 (±8%) kJ/mol. The lines in Fig. 3 *C* illustrate that Eq. 2 with the activation law for $k_{dark}(T)$ and the sum of the thermoactivated and temperature-independent contributions for $\alpha(T)$ can describe the experimental $\tau^{-1}(T)$ below T_{IF}.

DISCUSSION

Understanding the freezing process and frozen cells is of great importance for fundamental cryobiology and for practical cryopreservation tasks. One of the most significant effects that occurs in freezing cells is depression of their metabolic activity. We proposed to use the redox reaction rate of cytochromes as an indicator of frozen cell activity, and applied, to our knowledge, a new label-free approach

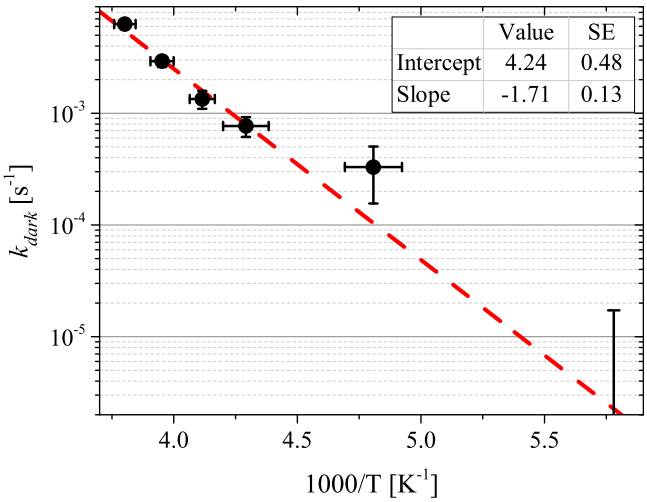

FIGURE 6 Temperature dependence of $k_{dark}(T)$ in the Arrhenius plot. At $T = -100°C$, the experimental value of k_{dark} is $0 \pm 1.7 \times 10^{-5}$ s^{-1} and only the upper limitation of k_{dark} is seen. The line is the fit by the thermal activation law ($R^2 = 0.98$). Error bars denote standard error. To see this figure in color, go online.

based on the photobleaching effect of the cytochrome resonance Raman lines to investigate the cytochrome redox balance and redox reaction rate. To our knowledge, this is the first study to examine cytochrome redox activity directly in freezing yeast cells. The important outcomes of our study are that 1) extracellular ice formation can result in the cytochrome reduction, and 2) the temperature dependence of the native redox reaction rates of cytochromes can be described by the thermal activation law.

The observed effects of ice formation on cytochrome reduction (Figs. 3 and S4) could be related, at least partially, to oxygen deficiency. After ice formation occurs, the cells become trapped inside small liquid brine inclusions (18) and all available oxygen is dissolved within the trap. Oxygen deficiency is believed to result in a reduction of cytochromes *b* and *c* via inactivation of the cytochrome oxidase complex (31,32). The increase in the reduced cytochrome concentration observed for aerated samples below T_{IF} (Fig. 3 *A*) can be explained by the slowdown of the electron flow in the ETC caused by anoxia. The same mechanism can explain the high concentration of the reduced cytochrome in nonaerated cells above T_{IF} (Fig. 3 *A*). This interpretation agrees with the low-temperature anoxia hypothesis (33).

Our experiments also show the temperature dependence of photoinduced and native redox reaction rates. The magnitude of these rates is determined by the chain of reactions involved in the redox balance. Effectively, if one step of the chain is much slower than the others, its reaction rate will determine the overall reaction rate of the chain. It appears that below T_{IF}, this slowest step demonstrates a strong temperature dependence on the photoinduced and native redox reaction rates (Figs. 3 and 5). However, above T_{IF}, these reaction rates are largely temperature independent (Fig. 3). This implies that ice formation at T_{IF} results in a change in the reaction rate of some ETC reactions. Although the exact reasons for this change are not clear, it could be explained by factors such as changes in the salt concentration, the effects of temperature on mitochondrial membranes and/or protein properties (34–37), anoxia effects, or changes in the metabolite concentration in solution (in the case of trapped cells). Further investigations are needed to clarify this point.

Below T_{IF}, the temperature dependencies $k_{dark}(T)$ and $\alpha(T)$ were described by the thermal activation law (Figs. 5, 6, and S5). The thermal activation energy for $\alpha(T)$, 21.3 kJ/mol, corresponds to the redox potential difference of ~220 mV, which is comparable to the standard reduction potential (160 mV) for the conversion of molecular oxygen to superoxide (38). The thermal activation law for $k_{dark}(T)$ implies that at temperatures below T_{IF}, the ETC is inactivated without any abrupt intermediate transitions, which potentially could be caused by changes in the protein conformations or mitochondrial membrane properties. The evaluated activation energy of $k_{dark}(T)$ (32.5 kJ/mol) is close to the energy of the phosphate bond of ATP, which is involved in the regulation of ETC activity (5,38). On the other hand, the activation energy of $k_{dark}(T)$ corresponds to the redox potential difference of ~340 mV, which is comparable to the potential redox differences in the ETC (38,39). However, it is challenging to unambiguously assign the ETC site that is responsible for the barrier of $k_{dark}(T)$.

The temperature dependence of the native redox reaction rate extracted from the photobleaching experiment sheds light on the slowdown of cellular activity in freezing cells. The characteristic time of the native reactions at liquid nitrogen temperature (−196°C) estimated from the activation law of Fig. 6 is $\sim 10^{17.7\ (\pm 2.2)}$ s, which is 10^{15} times higher than the time required at room temperature. If we consider cytochrome redox reactions as the representative process of cellular activity, we conclude that frozen cells can be stored in liquid nitrogen for $10^{10\ (\pm 2.2)}$ years. This evaluation exceeds the characteristic time of carbon exchange in Arctic bacteria, which is $\sim 10^8$ years at −40°C (40).

On the other hand, the proposed activation law (Fig. 6) implies a rapid shortening of the native redox reaction rate with increasing temperature (for example, τ is about 1000 years at −150 (±10)°C, 10 h at −80°C, 20 min at −40°C, and ~1 min at +25°C). The reaction rates extracted from the cytochrome photobleaching experiments can be used to predict the temperature dependence of the biological response in a particular cryopreservation protocol.

CONCLUSIONS

In this work, we studied the state and activity of the ETC in freezing yeast cells using a time-resolved resonance Raman approach. We showed that photobleaching of the resonance Raman lines is a useful tool for characterizing the redox

activity of cytochromes in cells. Our proposed label-free approach is universal and can be applied to study the effects of freezing on the ETC state in different aerobic life forms.

This study revealed that ice formation can influence the rate of cytochrome redox reactions and the balance between reduced and oxidized cytochromes. We propose that the cytochrome reduction results from low-temperature anoxia. We evaluated the temperature dependence of the rate of native redox reactions by conducting cytochrome photobleaching experiments. This rate was found to be well described by the thermal activation law with an apparent energy barrier of ~32.5 kJ/mol, demonstrating that the redox reaction rate at liquid nitrogen temperature is ~10^{15} times slower than that at room temperature.

Various biological processes are driven by the operation of the ETC. This study opens new avenues for obtaining contactless, label-free, single-cell characterizations of the ETC. Our method for measuring the rate of native redox reactions in situ can be extended to other applications as well, such as investigating the cell cycle, the effects of drugs on cell activity, and anoxia.

SUPPORTING MATERIAL

Supporting Materials and Methods, five figures, and one table are available at http://www.biophysj.org/biophysj/supplemental/S0006-3495(15)01108-X.

AUTHOR CONTRIBUTIONS

K.A.O. and N.V.S. designed the experiments, analyzed data, and wrote the manuscript. K.A.O. performed the experiments and analyzed raw data.

ACKNOWLEDGMENTS

The authors thank Y.V. Surovtseva for polishing the language of the manuscript.

This work was supported by the Russian Foundation for Basic Research (grant 14-04-31451).

SUPPORTING CITATIONS

References (41–45) appear in the Supporting Material.

REFERENCES

1. Stacey, G. N., and J. G. Day. 2014. Putting cells to sleep for future science. *Nat. Biotechnol.* 32:320–322.
2. Brinster, R. L. 2007. Male germline stem cells: from mice to men. *Science.* 316:404–405.
3. Amstislavsky, S. Y., and I. S. Trukshin. 2010. Cryobanking mammalian embryos: priorities and the optimal choice of reproductive technologies. *Russ. J. Dev. Biol.* 41:13–23.
4. Walters, C., P. Berjak, …, P. Raven. 2013. Plant science. Preservation of recalcitrant seeds. *Science.* 339:915–916.
5. Amato, P. 2013. Energy metabolism at low-temperature and frozen conditions in cold-adapted microorganisms. *In* Cold-Adapted Microorganisms. I. Yumoto, editor. Horizon Scientific Press, London, pp. 71–96.
6. Balcavage, W. X., J. C. Beck, …, J. R. Mattoon. 1970. Cryobiological studies of yeast mitochondria. *Cryobiology.* 6:385–394.
7. Mori, Y., H. Suzuki, and T. Nei. 1986. Freezing injury in the yeast respiratory system. *Cryobiology.* 23:64–71.
8. Yamanaka, M., S. Hashimoto, …, Y. Morimoto. 2011. Developmental assessment of human vitrified-warmed blastocysts based on oxygen consumption. *Hum. Reprod.* 26:3366–3371.
9. Dalcin, L., R. C. Silva, …, C. M. Lucci. 2013. Cytoskeleton structure, pattern of mitochondrial activity and ultrastructure of frozen or vitrified sheep embryos. *Cryobiology.* 67:137–145.
10. Amato, P., and B. C. Christner. 2009. Energy metabolism response to low-temperature and frozen conditions in *Psychrobacter cryohalolentis*. *Appl. Environ. Microbiol.* 75:711–718.
11. Atkin, O. K., Q. Zhang, and J. T. Wiskich. 2002. Effect of temperature on rates of alternative and cytochrome pathway respiration and their relationship with the redox poise of the quinone pool. *Plant Physiol.* 128:212–222.
12. David, P. S., and R. O. Poyton. 2005. Effects of a transition from normoxia to anoxia on yeast cytochrome *c* oxidase and the mitochondrial respiratory chain: implications for hypoxic gene induction. *Biochim. Biophys. Acta.* 1709:169–180.
13. Robertson, J. B., C. R. Davis, and C. H. Johnson. 2013. Visible light alters yeast metabolic rhythms by inhibiting respiration. *Proc. Natl. Acad. Sci. USA.* 110:21130–21135.
14. Chance, B., B. Schoener, …, Y. Nakase. 1979. Oxidation-reduction ratio studies of mitochondria in freeze-trapped samples. NADH and flavoprotein fluorescence signals. *J. Biol. Chem.* 254:4764–4771.
15. König, K., A. Uchugonova, and H. G. Breunig. 2014. High-resolution multiphoton cryomicroscopy. *Methods.* 66:230–236.
16. Thorell, B., B. Chance, and V. Legallais. 1965. Microspectrophotometry of cytochromes in the single cell at room and liquid nitrogen temperatures. *J. Cell Biol.* 26:741–746.
17. Dong, J., J. Malsam, …, A. Aksan. 2010. Spatial distribution of the state of water in frozen mammalian cells. *Biophys. J.* 99:2453–2459.
18. Okotrub, K. A., and N. V. Surovtsev. 2013. Raman scattering evidence of hydrohalite formation on frozen yeast cells. *Cryobiology.* 66:47–51.
19. Kreiner-Møller, A., F. Stracke, and H. Zimmermann. 2014. Hydrohalite spatial distribution in frozen cell cultures measured using confocal Raman microscopy. *Cryobiology.* 69:41–47.
20. Spiro, T. G., and T. C. Strekas. 1974. Resonance Raman spectra of heme proteins. Effects of oxidation and spin state. *J. Am. Chem. Soc.* 96:338–345.
21. Kakita, M., V. Kaliaperumal, and H. O. Hamaguchi. 2012. Resonance Raman quantification of the redox state of cytochromes *b* and *c* in-vivo and in-vitro. *J. Biophotonics.* 5:20–24.
22. Brazhe, N. A., M. Treiman, …, O. V. Sosnovtseva. 2012. Mapping of redox state of mitochondrial cytochromes in live cardiomyocytes using Raman microspectroscopy. *PLoS One.* 7:e41990.
23. Kakita, M., M. Okuno, and H. O. Hamaguchi. 2013. Quantitative analysis of the redox states of cytochromes in a living L929 (NCTC) cell by resonance Raman microspectroscopy. *J. Biophotonics.* 6:256–259.
24. Okada, M., N. I. Smith, …, K. Fujita. 2012. Label-free Raman observation of cytochrome *c* dynamics during apoptosis. *Proc. Natl. Acad. Sci. USA.* 109:28–32.
25. Walter, A., S. Erdmann, …, J. Popp. 2010. Analysis of the cytochrome distribution via linear and nonlinear Raman spectroscopy. *Analyst (Lond.).* 135:908–917.
26. Okotrub, K. A., and N. V. Surovtsev. 2014. Photobleaching of the resonance Raman lines of cytochromes in living yeast cells. *J. Photochem. Photobiol. B.* 141:269–274.
27. Mazur, P., and J. J. Schmidt. 1968. Interactions of cooling velocity, temperature, and warming velocity on the survival of frozen and thawed yeast. *Cryobiology.* 5:1–17.

28. Hu, S., I. K. Morris, …, T. G. Spiro. 1993. Complete assignment of cytochrome *c* resonance Raman spectra via enzymatic reconstruction with isotopically labeled hemes. *J. Am. Chem. Soc.* 115:12446–12458.

29. Jamieson, D. J. 1998. Oxidative stress responses of the yeast *Saccharomyces cerevisiae*. *Yeast.* 14:1511–1527.

30. Herrero, E., J. Ros, …, E. Cabiscol. 2008. Redox control and oxidative stress in yeast cells. *Biochem. Biophys. Acta.* 1780:1217–1235.

31. Guzy, R. D., and P. T. Schumacker. 2006. Oxygen sensing by mitochondria at complex III: the paradox of increased reactive oxygen species during hypoxia. *Exp. Physiol.* 91:807–819.

32. Ripple, M. O., M. Abajian, and R. Springett. 2010. Cytochrome *c* is rapidly reduced in the cytosol after mitochondrial outer membrane permeabilization. *Apoptosis.* 15:563–573.

33. Chan, K., J. P. Goldmark, and M. B. Roth. 2010. Suspended animation extends survival limits of *Caenorhabditis elegans* and *Saccharomyces cerevisiae* at low temperature. *Mol. Biol. Cell.* 21:2161–2171.

34. Watson, K., E. Bertoli, and D. E. Griffiths. 1975. Phase transitions in yeast mitochondrial membranes. The effect of temperature on the energies of activation of the respiratory enzymes of *Saccharomyces cerevisiae*. *Biochem. J.* 146:401–407.

35. McMurchie, E. J., and J. K. Raison. 1979. Membrane lipid fluidity and its effect on the activation energy of membrane-associated enzymes. *Biochim. Biophys. Acta.* 554:364–374.

36. Nardid, O., T. Dyubko, and S. Repina. 1997. A comparative study of the effect of freeze-thawing on peripheral and integral membrane proteins. *Cryobiology.* 34:107–113.

37. Wolkers, W. F., S. K. Balasubramanian, …, J. C. Bischof. 2007. Effects of freezing on membranes and proteins in LNCaP prostate tumor cells. *Biochim. Biophys. Acta.* 1768:728–736.

38. Nicholls, D. G., and S. J. Ferguson. 2013. Bioenergetics. Academic Press, London.

39. Dutton, P. L., D. F. Wilson, and C.-P. Lee. 1970. Oxidation-reduction potentials of cytochromes in mitochondria. *Biochemistry.* 9:5077–5082.

40. Price, P. B., and T. Sowers. 2004. Temperature dependence of metabolic rates for microbial growth, maintenance, and survival. *Proc. Natl. Acad. Sci. USA.* 101:4631–4636.

41. De Gelder, J., K. De Gussem, …, L. Moens. 2007. Reference database of Raman spectra of biological molecules. *J. Raman Spectrosc.* 38:1133–1147.

42. Mayo, D. W., F. A. Miller, and R. W. Hannah. 2004. Course Notes on the Interpretation of Infrared and Raman Spectra. John Wiley & Sons, Hoboken, NJ.

43. Prescott, B., W. Steinmetz, and G. J. Thomas, Jr. 1984. Characterization of DNA structures by laser Raman spectroscopy. *Biopolymers.* 23:235–256.

44. Pliss, A., A. N. Kuzmin, …, P. N. Prasad. 2010. Nonlinear optical imaging and Raman microspectrometry of the cell nucleus throughout the cell cycle. *Biophys. J.* 99:3483–3491.

45. Uzunbajakava, N., A. Lenferink, …, C. Otto. 2003. Nonresonant Raman imaging of protein distribution in single human cells. *Biopolymers.* 72:1–9.

Supporting Material

"Redox state of cytochromes in frozen yeast cells probed by resonance Raman spectroscopy"

Konstantin A. Okotrub and Nikolay V. Surovtsev*

*Corresponding author, email: lab21@iae.nsk.su

Pr. Ak. Koptyuga 1, 630090, Novosibirsk, Russia

Tel. 7-383-3307978

Raman lines assignment

In our Raman experiment the yeast cell suspension was placed between two silica glass plates or between a glass plate and a piece of mica (Materials and Methods of Article). Hence, Raman signal from the mica slice and/or the silica glass can contribute to the measured Raman spectra. To take into account these contributions the Raman scattering from the silica glass and the mica slice was studied. Raman spectra of the yeast cell in the sample installation, the silica glass and the mica slice measured at different temperatures are shown in Fig. S1. Figure S1 helps in the assignment of the experimental Raman lines. From Fig. S1 it is seen that the Raman spectra of the mica and silica weakly depend on temperature.

Raman spectrum of yeast cells averaged over the different scan during the measurements is shown in Fig. S1 at few representative temperatures. Temperature evolution of Raman spectrum relates to the change of the cytochrome contribution discussed in Article. Non-resonance Raman lines obey weak temperature dependences (Fig. S1). The assignment of Raman lines corresponding to the yeast cell is presented in Table S1.

Photoluminescence background in the measured spectra was corrected with a straight line. At room temperature the intensity of photoluminescence was

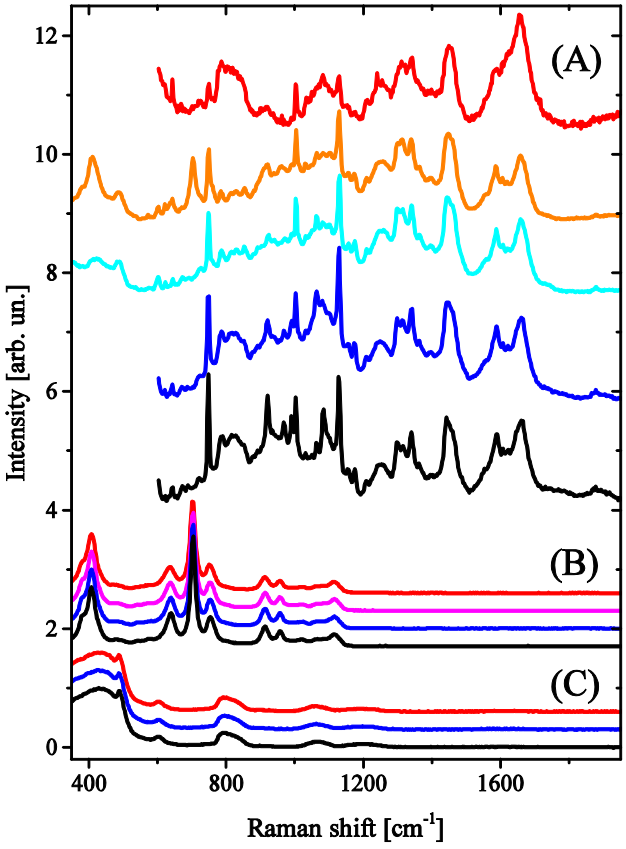

FIGURE S1. (*A*) Raman spectra of yeast cells in the sample installation of the Linkam cryostage at T = -30 °C (the orange line) and in the sample installation of the vacuum cryostat at T = +25 °C (the red line), -70 °C (the cyan line), -100 °C (the blue line), -173 °C (the black line). (*B*) Raman spectra of a mica slice at T = +25, -30, -100, -180 °C (from top to bottom). (**C**) Raman spectra of a silica glass at T = +25, -40, -170 °C (from top to bottom). The spectra are vertically shifted for convenience.

somehow lower than the intensity of CH deformation mode. At -100 °C the photoluminescence was 50 times more intensive than at room temperature (for the first scan with 2 min exposition). However, the laser exposition leads to the photoluminescence background decrease. At -100 °C the photoluminescence decreases under irradiation by more than an order of magnitude.

TABLE S1. Raman lines assignment.

Line position, cm^{-1}	**Assignment**
604	cytochrome *c* (1, 2)
622	phenylalanine (3)
645	tyrosine (3)
672	thymine (5)
688	cytochrome (2); guanine (5)
724	adenine (5)
749	cytochrome *c* and *b* (2)
786	cytosine, thymine (5)
814	RNA phosphate backbone (5,6)
830	phenylalanine (3)
852	tyrosine (3)
879	undetermined: possibly phosphate backbone (5)
892, 905	rocking CH_2 (3,4)
922, 970, 992	cytochrome *c* and *b* (2)
1004	phenylalanine (3,7)
1032	phenylalanine (3,7)
1050	C - O (4,5)
1064, 1081, 1102	saturated compounds (C-C) (3)
1129, 1155, 1176	cytochrome *c* and *b* (2)
1210	phenylalanine, tyrosine (7)
1250 (broad)	saccharides, aminoacides, nucleotides (3)
1300	twisting CH_2 (3); cytochrome *c* and *b* (2); amide III (4,7)
1315, 1341	cytochrome *c* and *b* (2)
1392	deoxyribose phosphate backbone $\delta(CH_2)$, guanine (3,5)
1450 (broad)	scissoring CH_2, umbrella CH_3 modes (4)
1552	amide II (4)
1587	cytochrome *c* and *b* (2); phenylalanine (3)
1606, 1619	undetermined: C = C or aromatic C ⋯ C (4)
1655 (multicomponent)	amide I (1650 cm^{-1}) and other C = O, C = C (4)
1734, 1877	C = O (4)

Data processing

We followed the intensity ratio of 749 cm^{-1} and δCH Raman lines to estimate the reduced cytochrome amount in yeast cells. The way of the line intensities estimation is illustrated in Fig. S2. Intensity of the cytochrome peak at 749 cm^{-1} was quantified as a difference between the average of three pixels of maximal intensity and the baseline.

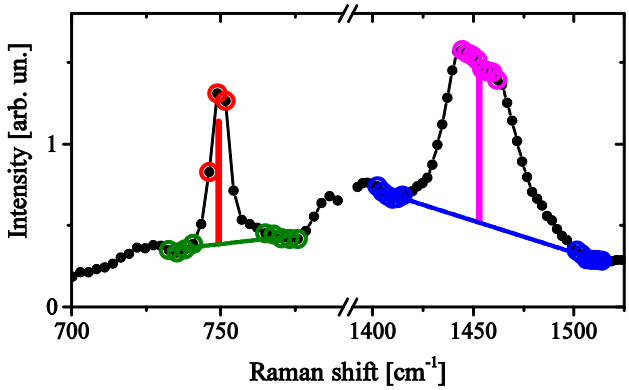

FIGURE S2. Quantification of the yeast Raman line intensities. The green and blue points denote the pixels used in the baseline interpolation, which are shown by the straight lines. The vertical lines demonstrate the intensity of the peaks quantified as described in the text.

The baseline was interpolated by a straight line between the pixels determining the peak background (Fig. S2). The similar calculations were used for the δCH mode (see Fig. S2), where the average of nine pixels of maximal intensity were used. This is equivalent to integration range of ~27 cm^{-1}. The integration range minimizes the effect of temperature for the δCH mode (see Fig. 2 of Article). Where necessary the overlap of the cytochrome peak at 749 cm^{-1} with the mica spectrum was taken into account (the typical correction value was less than 10 % of the value of 749 cm^{-1} line at the beginning of the irradiation).

From 10 to 40 cells were studied at all considered experimental conditions depicted in Figs. 3 and 4 of Article. For every cell the experimental

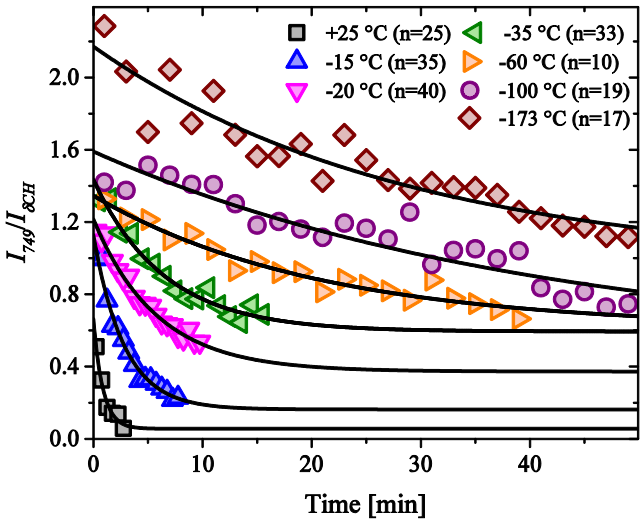

FIGURE S3. Time dependence of the $I_{749}/I_{\delta CH}$ ratio at different temperatures (P = 2.4 mW). Not all data are shown for the experiment at T = -100, -173 °C; the total exposition time was 80 minutes in this case. The number of cells used in averaging is shown in brackets.

$I_{749}/I_{\delta CH}$ (t) ratio was fitted with decaying exponent (see Eq. 1). The average values of the parameters (τ^{-1}, $y0$, A) discussed in Article were found from the arithmetical mean over the set of parameters of different cells. To verify the validity of the exponential decay fit the $I_{749}/I_{\delta CH}$ (t) ratio with higher statistics was considered. In this case the $I_{749}/I_{\delta CH}$ (t) ratio was found from averaging over Raman spectra of all cells studied. The time dependence of this ratio is shown in Fig. S3 at a few representative temperatures. It is seen that the exponential decay fit works well.

Effect of ice formation

In one experiment the spontaneous ice formation occurred only after ~2 hours of being at -20 °C. Raman scattering measurement from single cells had been started before the ice formation and finished after that (Fig S4). The Raman measurement from the first 16 cells was done from the cells contained in supercooled solution. In this case the ratio $I_{749}/I_{\delta CH}$ was about 0.1 for 4 minutes acquisition. After the ice formation the Raman measurements were performed from the cells trapped in the ice. The first one of them showed the $I_{749}/I_{\delta CH}$ ratio similar to one measured before. Next measurements provided the average $I_{749}/I_{\delta CH}$=1.3. Fig. S4 demonstrates the effect of the spontaneous ice formation on the intensity of the cytochrome contribution. We estimated that the process of cytochrome reduction in cells had taken from 5 to 10 minutes.

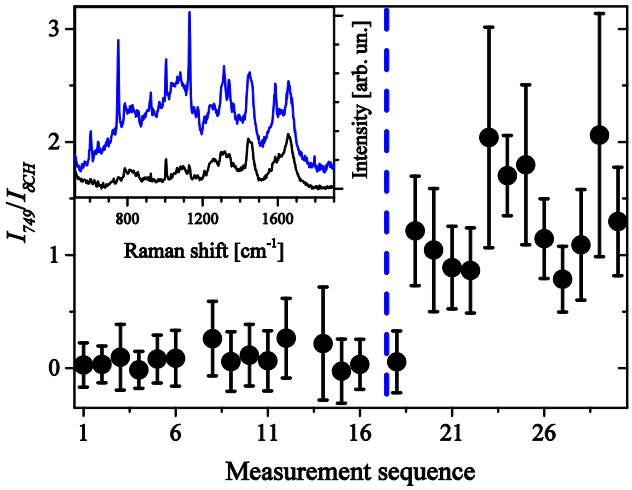

FIGURE S4. Effect of the ice formation on $I_{749}/I_{\delta CH}$ ratio at T = -20 °C. The black circles correspond to $I_{749}/I_{\delta CH}$ ratio evaluated from the single cell measurements with 4 minutes exposition. The vertical line depicts the moment of ice formation in the experiment. The insert: the Raman spectra measured before and after ice formation.

Arrhenius plot for α coefficient

Temperature dependence of the α coefficient from Eq. (2) can be described by the sum of the thermal activation law and a constant, see Fig. 5.

$$\alpha(T) = \alpha_0 + q_0 e^{-U/T} \qquad \textbf{(Eq. S1)}$$

The activation energy of $\alpha(T)$ of 21.3 (±15%) kJ/mol and the constant contribution α_0 of 8 (±0.5)·10^{-5} $s^{-1}mW^{-2}$ was determined from the fit (Figs. 5 and S5). Fig. S5 shows the Arrhenius plot for the $\alpha(T)$ coefficient with the constant contribution subtracted.

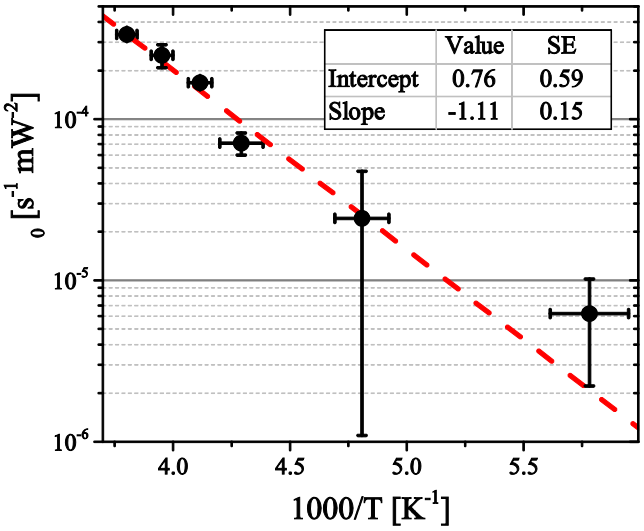

FIGURE S5. Arrhenius plot of the α coefficient with the constant contribution (α_0) subtracted. The line is the fit by the thermal activation law ($R^2 = 0.98$). Error bars denote standard error.

SUPPORTING REFERENCES

1. Kakita, M., V. Kaliaperumal, and H. Hamaguchi. 2012. Resonance Raman quantification of the redox state of cytochromes b and c in-vivo and in-vitro. *J. Biophotonics.* 5:20–24.

2. Hu, S., I. K. Morris, …, T. G. Spiro. 1993. Complete assignment of cytochrome c resonance Raman spectra via enzymatic reconstruction with isotopically labeled hemes. *J. Am. Chem. Soc.* 115:12446–12458.

3. De Gelder, J., K. De Gussem, …, L. Moens. 2007. Reference database of Raman spectra of biological molecules. *J. Raman Spectrosc.* 38:1133–1147.

4. Mayo, D. W., F. A. Miller, and R. W. Hannah. 2004. Course Notes on the Interpretation of Infrared and Raman Spectra. John Wiley & Sons, Hoboken, NJ.

5. Prescott, B., W. Steinmetz, and G. J. Thomas, Jr. 1984. Characterization of DNA structures by laser Raman spectroscopy. *Biopolymers.* 23:235–256.

6. Pliss, A., A. N. Kuzmin, …, P. N. Prasad. 2010. Nonlinear optical imaging and Raman microspectrometry of the cell nucleus throughout the cell cycle. *Biophys. J.* 99:3483–3491.

7. Uzunbajakava, N., A. Lenferink, …, C. Otto. 2003. Nonresonant Raman imaging of protein distribution in single human cells. *Biopolymers.* 72:1–9.